Parallel Motions of Coronal Hard X-ray Source and Hα Ribbons

Jeongwoo Lee and Dale E. Gary

Physics Department, New Jersey Institute of Technology, Newark, NJ 07102

ABSTRACT

During solar flares Hα ribbons form and often move away from the local magnetic polarity inversion line (PIL). While the motion perpendicular to the PIL has been taken as evidence for coronal magnetic reconnection in the so-called CSHKP standard model, the other velocity component parallel to the PIL is much less adopted as a property of the magnetic reconnection process. In this Letter we report an event in which the motion parallel to the PIL is found in both Hα ribbons and a thermal hard X-ray source. Such commonality would indicate a link between the coronal magnetic reconnection and footpoint emissions as in the standard solar flare model. However, its direction implies a reconnection region that is increasing in length, a feature missing from the standard two-dimensional model. We present a modified framework in which the variation along the third dimension is allowed, in order to assess the effect of such a proper motion on estimation of the magnetic reconnection rate. Data used are hard X-ray maps from the *Reuven Ramaty High Energy Solar Spectroscopic Imager* (*RHESSI*), Hα filtergrams of Big Bear Solar Observatory (BBSO), and the *SOHO* Michelson Doppler Imager (MDI) magnetogram obtained for the 2004 March 30 flare.

Subject headings: Sun: flares — Sun: magnetic fields

1. Introduction

Hα ribbons forming during solar flares are thought to be due to precipitation of energetic particles accelerated in the corona (Kane & Donnelly, 1971) in which case their morphology serves as a direct mapping of the coronal magnetic reconnection geometry into the chromosphere (Priest & Forbes 2002). This can be applied to infer the coronal magnetic reconnection rate from the temporal change of the magnetic flux measured within the area of Hα ribbons, $\dot{\phi} = (\partial/\partial t) \int B \, da$, where B is the magnetic field component normal to the surface element da. Forbes & Priest (1984) noticed that $\dot{\phi}$ is equivalent to the electric potential drop along the coronal separator, $V = \int E \, dl$, if the specific two-dimensional (2D) model

applies. Here E is electric field and dl is a length element along the separator in the corona. The equation $\dot{\phi} = V$ then reduces to an expression for the electric field, $E = uB$, where u is the ribbon separation velocity. This formulation, enabled under the standard 2D model, is important because it permits calculation of the two key parameters (E, V) characterizing the invisible coronal reconnection from observations of the chromospheric features, (uB, $\dot{\phi}$).

To evaluate the framework, we need another observable quantity that can serve as an independent measure for the magnetic reconnection. Hard X-ray (HXR) emission is considered adequate for this purpose, because it well represents the rate of energy deposition, ϵ, by energetic electrons, the primary portion of the magnetic energy release. Since this functionality of HXR as a particle signature is very different from that of Hα ribbons as a direct indicator of coronal dynamics, any correlation found between them can be good evidence for the reconnection model. The first result of such comparisons (Qiu et al. 2002) successfully showed that the magnitude of uB has a temporal correlation with HXR lightcurves. Soon after, Asai et al. (2002) pointed out that additional constraints can be imposed for the spatially resolved footpoint motion: (1) only the velocity component perpendicular to the PIL should be related to the reconnection rate under the standard model, and (2) the local ribbon velocity and local energy release rate may depend on the local field strength as $u \sim B$ and $\epsilon \sim B^3$ if Petschek's (1964) reconnection theory is incorporated into the standard model. It thus appears that not only uB but u itself can serve as constraints on the standard 2D model.

Temporally, the above two relationships imply $u \sim \epsilon^{1/3}$, namely, HXR sources should move fast during the flare maximum phase and slowly at other times. An episodic variation of ribbon motion with the HXR light curves found by Lee et al. (2006) does support this idea. However, there are also counter examples: Krucker et al. (2003) found a correlation of HXR light curves with parallel, rather than perpendicular, motions of HXR sources with respect to the PIL. Grigis & Benz (2005) reported an event in which neither the perpendicular nor the parallel motions of HXR sources correlates with HXR lightcurves. Spatially, the proposed relationship $\epsilon \sim B^3$ was supported by studies of HXR source locations along Hα ribbon axes (Miklenic et al. 2007; Temmer et al. 2007). However, another study on spatially-resolved ribbon velocity found rather an anticorrelation between u and B (Jing et al. 2007, 2008). Similarly, it is our common experience that separation of HXR sources is usually much less than that of Hα ribbons, counter to the above prediction.

With these nonstandard dynamic behaviors of Hα ribbons and HXR footpoint sources, the proposed relationship, $\dot{\phi} \equiv V$, may need to be revisited. How closely $\dot{\phi}$ will reproduce V depends on how good an approximation the standard 2D model is to the actual, complex magnetic reconnection process (for a general formulation of magnetic reconnection, see Hesse

et al. 2005). This makes it important to check whether the nonstandard behaviors imply another degree of freedom not included in the 2D model and, if so, how such motions can be incorporated into estimates of the reconnection rate. It is also important to observe not only the chromospheric features but their coronal counterparts, since the issue is how to test the ability to predict coronal physics based on the chromospheric signatures. In this Letter we present a simple formulation for the 3D reconnection and apply it to a two-ribbon flare. In most flares, the coronal and footpoint HXR sources are simultaneously observed with a tendency that the former dominates in weaker events. Since our focus is the relative motion of the coronal source and the chromospheric ribbon motions, we use a modest two-ribbon flare on 2004 March 30 which shows only the coronal HXR source.

2. Formulation

In order to incorporate the length variation of the coronal reconnection region into the standard 2D model, we start from the principle of magnetic flux conservation in 3D. For simplicity we consider a rectangular coronal region with area LW connected to another rectangular area in the chromosphere with area lw via field lines, as shown in Figure 1. Here, the lengths (l, L) are measured parallel to the PIL and the widths (w, W), perpendicular to the PIL. We then have

$$B_c LW = Blw, \tag{1}$$

where B_c is the coronal magnetic field and B the photospheric field. This reduces to the usual expression, $E \equiv \dot{W} B_c = u_{\parallel} B$ in the case of translational symmetry along a magnetic arcade, $L = l$, and otherwise shows how the electric field would be affected by the length variation of Hα ribbons. Taking a time derivative of both sides of this equation and rearranging them, we find the parallel electric potential along the separator as

$$V \equiv EL = \dot{W} B_c L = \dot{\phi} - (\dot{L}/L)\phi. \tag{2}$$

The last term is the correction term for the 3D effect in this case. The 2D model represents one extreme case that the above correction term vanishes and the measured $\dot{\phi}$ is equivalent to the coronal electric potential V. The other extreme case is possible when the flux change rate is entirely due to increasing L, e.g., the trigger moves along the ribbon without ribbon separation (cf. Grigis & Benz 2005). In this case there would be no electric field involved with the observed flux change rate ($V = 0, \dot{\phi} > 0$). In the intermediate case ($0 < V < \dot{\phi}$) this relation can tell the difference between the parallel electric potential V and the measured flux change rate $\dot{\phi}$ in terms of the logarithmic time variation of the coronal length $\dot{L}/L$ and magnetic flux ϕ measured during a reconnection event.

3. Observation and Interpretation

A modest two-ribbon flare occurred on 2004 March 30 in AR10581 near disk center, S04W03 (49",42"), at 22:53 UT, acquiring *GOES* class C2.0. We produce HXR maps from the *Ramaty High Energy Solar Spectroscopic Imager* (*RHESSI*) data in 5–20 keV with 2 minute time cadence in accordance with that of the Hα images from the Big Bear Solar Observatory (BBSO). A single *SOHO*/Michelson Doppler Imager (MDI) magnetogram taken at 22:28 UT is used for the line-of-sight magnetic fields.

3.1. Radiation Intensity and Magnetic Field

Figure 2 shows the spatial distributions of Hα intensity and local magnetic field along the ribbon axes. The top left panel shows the Hα ribbon axes (*red lines*) and HXR axes (*blue lines*) on a Hα image. We define the ribbon axes by the locations of the local maximum intensity at a given direction normal to the nearest PIL. The HXR axis is determined based on the shape of the source elongation. In the remaining panels, the intensity profiles along the axes are shown in 1D forms with the coordinates given in units of arc-seconds, centered at the location of peak intensity, and increasing from the south to the north. The local magnetic field (*black lines*) is shown for comparison with Hα intensities, and not shown for the HXR coronal source as it is unavailable in this case. We can see that the brighter sections of Hα (*gray shaded areas* representing $\geq$50% of their maxima at each time) encompass the local strong field regions. This spatial correlation between Hα brightness and local magnetic field strength is similar to that found between HXR footpoints and strong magnetic field in previous studies (Asai et al. 2002; Jing et al. 2007), except that these Hα peaks are much broader than the local magnetic field strength distribution. The latter is expected due to the complicated response of Hα radiations to input heating (Gayley & Canfield 1991). The spatial correlation of Hα intensity with local magnetic field is consistent with the idea of the primary energy release via magnetic reconnection and the strong dependence of the magnetic reconnection rate on local field strength as predicted by the 2D model (see §1).

However, we would like to point out that the location of the brighter Hα section could simply be explained by the principle of magnetic flux conservation in 3D as given in equation (1) or shown in Figure 1. Supposing that the magnetic energy is released more or less uniformly over the coronal region of interest, we will see the flare radiation appear brighter over a stronger field region as it collects energy from a wider coronal area. The enhancement is given by the area ratio LW/lw, which is proportional to B.

3.2. Motions of the HXR source and Hα Ribbons

Figure 3 shows the Hα and HXR coronal sources as contours overlaid on the magnetogram. The radiation sources at each time interval are shown as a single contour level at 50% of the maximum intensity of each source. The PIL on the magnetogram is shown as the dot-dashed line. It shows that this active region has one dominating round spot in the west and the other polarity fields are scattered around in the east. Accordingly, the Hα ribbon in the positive polarity is more elongated than the one in the negative polarity near the sunspot. Such apparent asymmetry is common and would not necessarily preclude the applicability of the 2D model, since the ribbon geometry relative to the PIL is topologically equivalent to the standard model.

From the successive change of HXR contours, we can see the HXR source move nearly parallel to the PIL. This motion is not obvious at the very peak time of the flare ∼23:00 UT and becomes obvious on and after 23:03 UT. It is northward rather than being symmetrically bidirectional. Interestingly, Hα ribbon 1 also extends northward parallel to the PIL in addition to its motion away from the PIL. The Hα expansion along its length is, in fact, more obvious in a movie, where it appears as a bright blob moving along the ribbon. Ribbon 2 is also expected to show a countermotion but is too compact to show such a motion clearly. From the time-dependent change of the boundary of ribbon 1 (*contours* in Fig. 3), we estimate $u_\perp \approx 24$ km s^{-1} and $u_\parallel \approx 47$ km s^{-1} on average. Thus, the parallel expansion of the ribbons is about twice as fast as the perpendicular separation between them and is also more obvious in the later phase. The common direction of motion shared by both the Hα and coronal HXR source convinces us that the Hα ribbon expansion is directly connected with the primary energy release in the corona rather than merely a secondary process in the chromosphere.

3.3. Ribbon Motion and Magnetic Field

It is tricky to measure the local velocities within an Hα ribbon unless traceable elements are found inside the ribbons. As one way, we may determine the axes of the Hα ribbon 1 by the locations of the local maximum intensity as shown in the left panel of Figure 4. The successive displacement of the ribbon axes with time shows a tendency that $u_\perp$ is larger in regions of weaker magnetic field. For instance, regions A and C have weak fields where the ribbon sections move fast. On the other hand, region B has strong magnetic fields where the ribbon moves little. The northern tip of the ribbon slows down as it approaches the strong field. Therefore, the ribbon separating motion is rather inversely proportional to local magnetic field strength in this case. This behavior is similar to the anticorrelation of

ribbon motion with the local magnetic field strength found by Jing et al. (2007, 2008).

If we alternatively define the ribbon motion in terms of the foremost front of the ribbon (*right panel* in Fig. 4), the impression changes. Especially, in region B, the ribbon edge moves quite fast unlike the above-noted dynamical behavior of the ribbon axis. However, even in this case, the motion is fast in the vicinity of the local strong field region rather than exactly in the strong field region.

Equation (1) can also account for the velocity anti-correlating with the local magnetic field, because a change in the coronal area, ΔLW is not solely reflected by the corresponding increment in the chromospheric width, $\triangle w$, but depends on other terms: Δl and B/B_c. This explanation is not possible in the 2D model, because the 2D model allows no degree of freedom along the PIL and any coronal change should strictly be reflected in the distance perpendicular to the PIL.

3.4. Parallel Electric Potential

To determine how much V differs from $\dot{\phi}$ using equation (2) the logarithmic time variation of the length of the reconnection region, $\dot{L}/L$, should be known. Unfortunately L and $\dot{L}$ are not directly measurable. Here we will assume $\dot{L}/L \approx \dot{l}/l$. This approximation is expected to be good when the mapping of L onto l is almost linear. Namely, if L is always larger than l by a constant factor, then $\dot{L}$ will also be larger than $\dot{l}$ by the same factor. The $\dot{L}/L$ determined in this way is plotted in the left panel of Figure 5 together with other parameters associated with the correction term. While $\dot{L}/L$ decreases with time, ϕ increases and thus the correction term $(\dot{L}/L)\phi$ remains nearly constant and significant in this event. The right panel shows our predictions for electric potential and field in comparison with the measured flux change rate. After the correction, the maximum electric voltage reduces to 57% of the maximum flux change rate $\approx 5.3\times10^{17}$ Mx s^{-1}. Temporally, the electric potential V drops to zero as early as $\lesssim$6 minutes after the maximum intensity whereas the apparent flux change rate $\dot{\phi}$ remains at a significant level for a much longer time. Likewise, the *average* electric field, $E = V/L$, is sustained over a shorter period than implied by the observed time profile of the flux change rate $\dot{\phi}$. Depending on the correction term, the peak electric field may come earlier than the peak magnetic flux change rate, which is not obvious in this case due to the small number of data points.

4. SUMMARY

The present study demonstrates some aspects of solar magnetic field reconnection that have not been discussed before. (1) The locations of HXR sources (or, as a proxy, bright Hα ribbons) in the stronger magnetic field section of ribbons has been regarded as evidence for the standard model (Asai et al. 2002; Miklenic et al. 2007; Temmer et al. 2007). We however suggest that this phenomenon could simply be explained by the rapid convergence of field lines from a coronal energy release region into a strong field region in the chromosphere. (2) Our formulation shows that a fast change in the coronal area does not necessarily result in a larger increment in the chromospheric width, as it also depends on the length variation. This may account for the weak anticorrelation of ribbon motion with the local magnetic field strength found by Jing et al. (2007, 2008). (3) The observed flux change rate has thus far been treated as equivalent to the coronal electric voltage following the standard 2D model, while there could be a difference between them in the realistic 3D reconnection. A more general relationship between them is presented here to accommodate the time-dependent change of Hα ribbon lengths. This relationship may be too simple to serve as a quantitative tool, but at least it analytically explains why HXR lightcurves are more impulsive than inferred by perpendicular Hα ribbon motions in some events. This alternative framework reduces to the standard model in 2D-like events and complements it when the length variation of the reconnection region is indicated by observations.

We thank our referee, Säm Krucker, for many comments, and Chang Liu for help with the RHESSI data. We were supported by NSF grant AST 06-07544 and NASA grant NNG0-6GE76G.

REFERENCES

Asai, A., Masuda, S., Yokoyama, T., Shimojo, M., Isobe, H., Kurokawa, H., & Shibata, K., 2002, ApJ, 578, L91

Forbes, T.G. and Priest, E.R.: 1984, in Solar Terrestrial Physics: Present and Future, ed. D.M. Butler, K. Papadopoulous (NASA RP-1120, Washington, D.C.) p 1

Gayley, K. G. & Canfield, R. C. 1991, ApJ, 380, 660

Grigis, P. C., & Benz, A. O., 2005, ApJ, 625, 143

Hesse, M., Forbes, T. G., & Birn, J., 2005, ApJ, 631, 1227

Jing, J., Lee, J., Liu, C., Gary, D. E., & Wang, H. 2007, ApJ, 664, L127

Jing, J., Chae, J., & Wang, H. 2008, ApJ, 672, 73

Kane, S. R. & Donnelly, R. F. 1971, ApJ, 164, 151

Krucker, S., Hurford, G. J., & Lin, R. P., 2003, ApJ, 595, L103

Lee, J., Gary, D. E., & Choe, G. S., 2006, ApJ, 647, 638

Miklenic, C. H., Veronig, A. M., Vršnak, B., & Hanslmeier, A., 2007, A&A, 461, 697

Petschek, H. E. 1964, in Solar Flares, ed. W. N. Hess (NASA SP-50; Washington, DC: NASA), 425

Priest, E. R. & Forbes, T. G. 2002, A&ARv, 10, 313

Qiu, J., Lee, J., Gary, D. E., & Wang, H. 2002, ApJ, 565, 1335

Temmer, M., Veronig, A. M., Vršnak, B., & Miklenic, C., 2007, ApJ, 654, 674

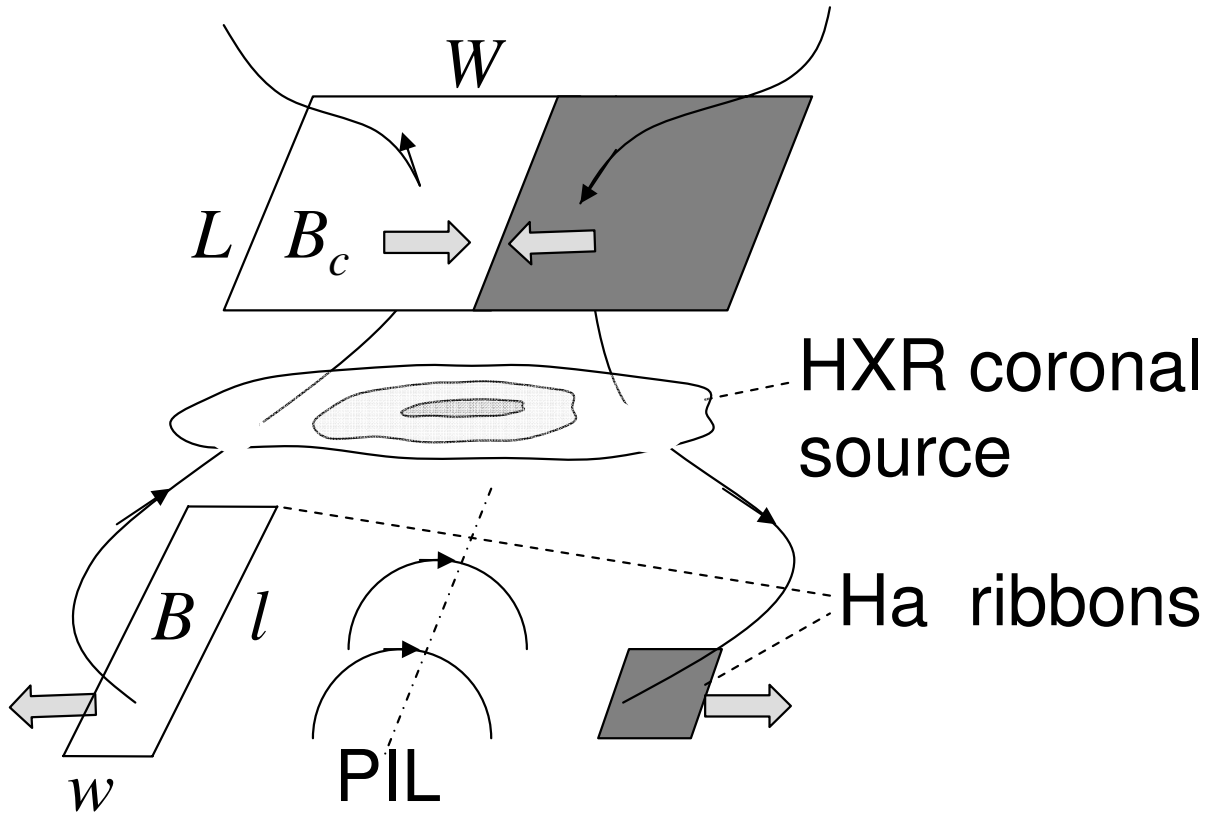

Fig. 1.— Magnetic field configuration used in the formulation. The curved lines are field lines with each magnetic polarity indicated with arrows. The lower two rectangular boxes are flare ribbons, and the upper two adjacent rectangles are the connected regions in the corona. For instance, one ribbon with magnetic field B and area lw is connected to the coronal region with field B_c and area LW. The block arrows show separating footpoint motion in the chromosphere and incoming motion in the coronal reconnection region.

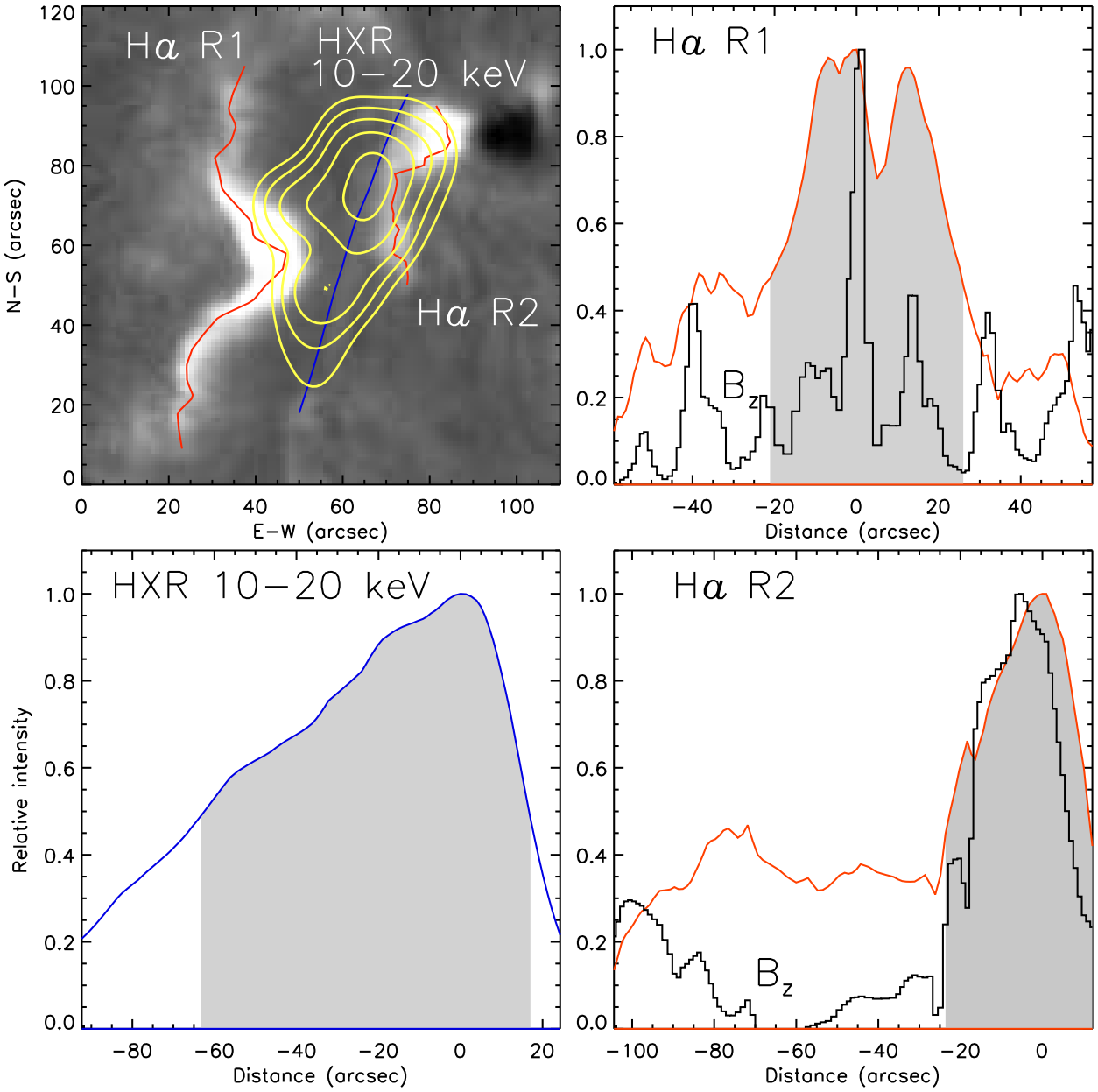

Fig. 2.— Spatial distributions of Hα and HXR intensities during the 2004 March 30 flare. Top left panel shows Hα ribbon axes and the coronal HXR source axis overlaid on the Hα image (*gray scale*) at 23:06:51 UT. The yellow contours represent the coronal HXR source. The other panels show 1D profiles of Hα and HXR intensities read along their axes. The ribbon intensities are compared with local magnetic field and the gray areas represent the section of each source brighter than 50% of its maximum intensity.

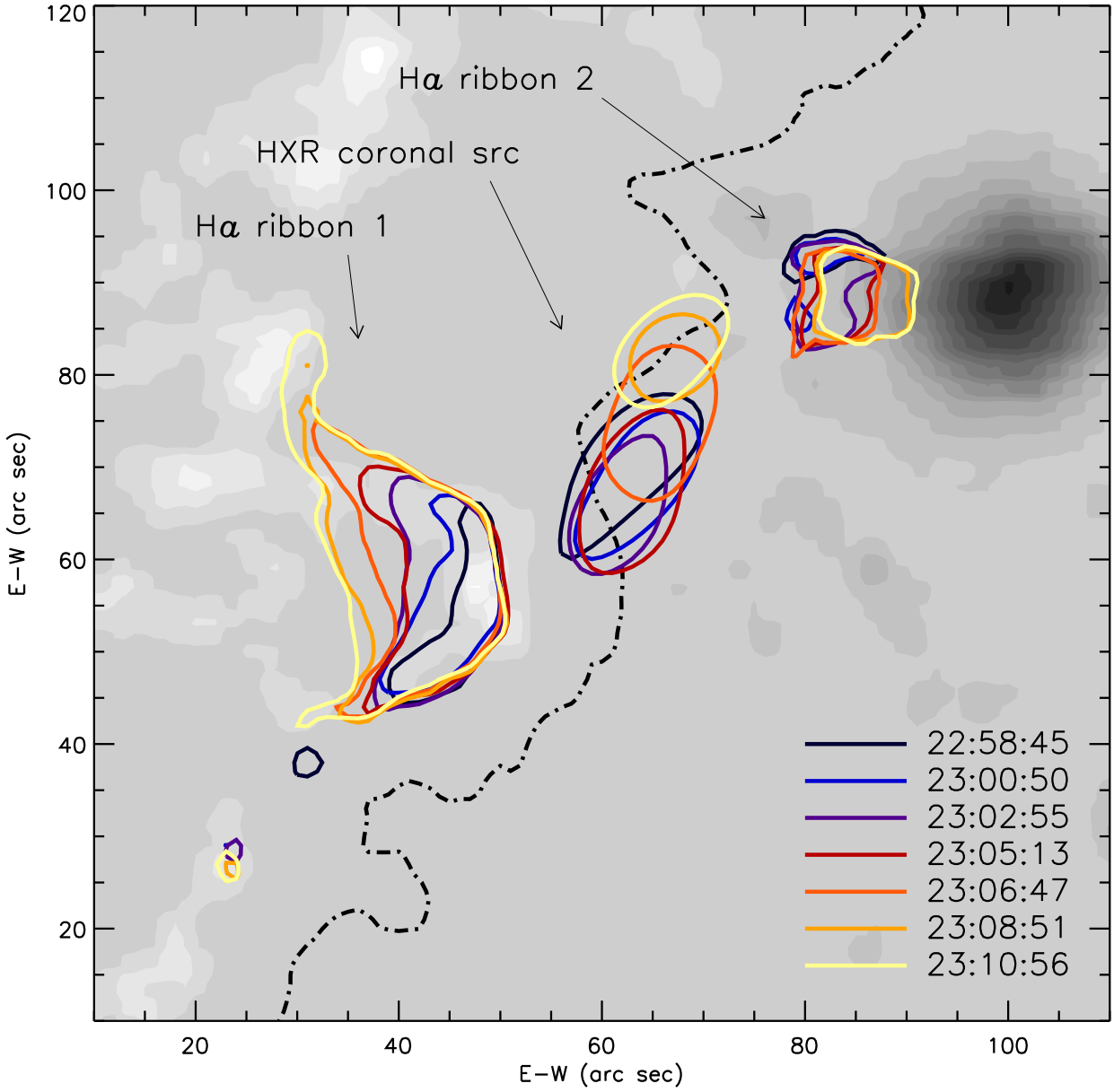

Fig. 3.— Motions of the coronal HXR source and Hα ribbons. The radiation sources are shown as contours. Only a single contour level (50% of the maximum intensity of Hα ribbons and 90% of the HXR source) is shown at each time with the color code. The color, changing from black to yellow, indicates a 12 minute time lapse from 22:58 to 23:12 UT with roughly 2 minute cadence. The gray-scale image is the line-of-sight magnetogram from *SOHO*/MDI taken at 22:28 UT.

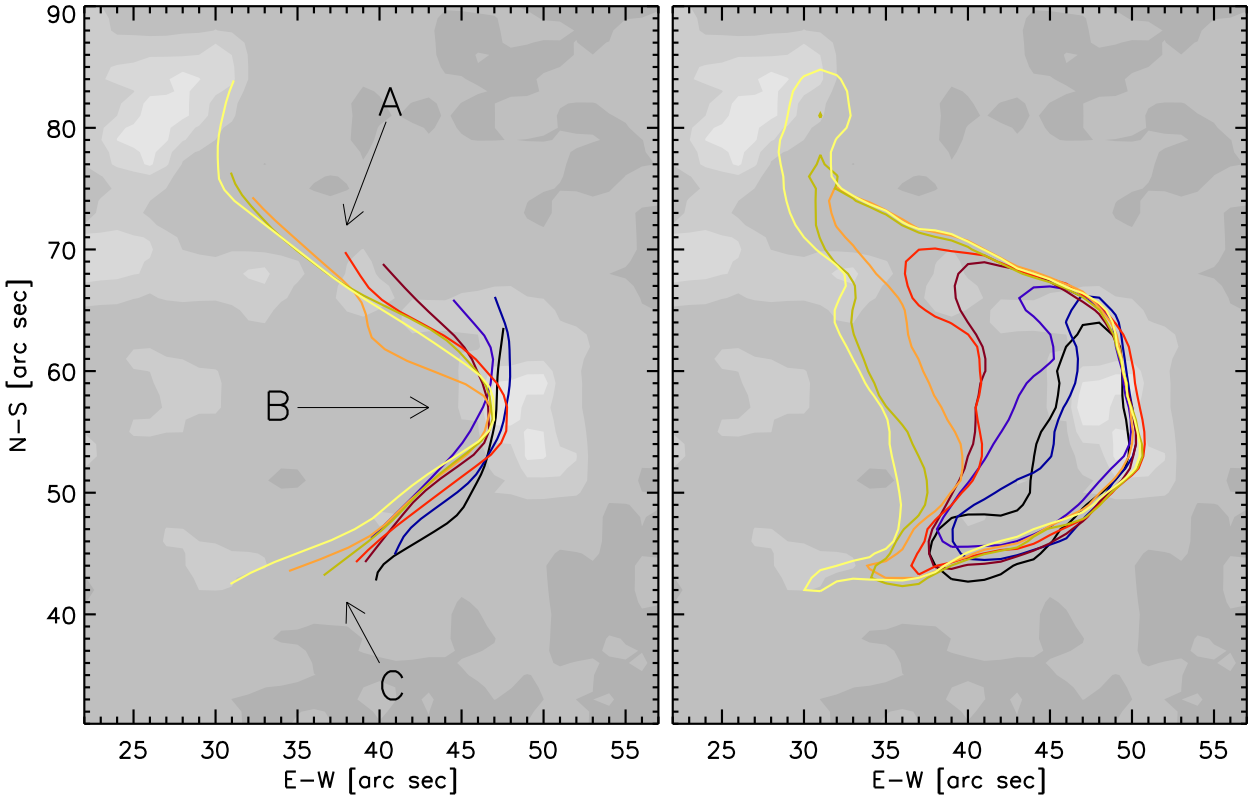

Fig. 4.— Traces of the Hα ribbon 1 at six time intervals overlaid on the MDI magnetogram. The same color code for time intervals as in Fig. 3 is used. *Left*: Ribbon axes determined by local maximum intensity. *Right*: Ribbon boundaries defined by 50% of the maximum intensity at individual time intervals.

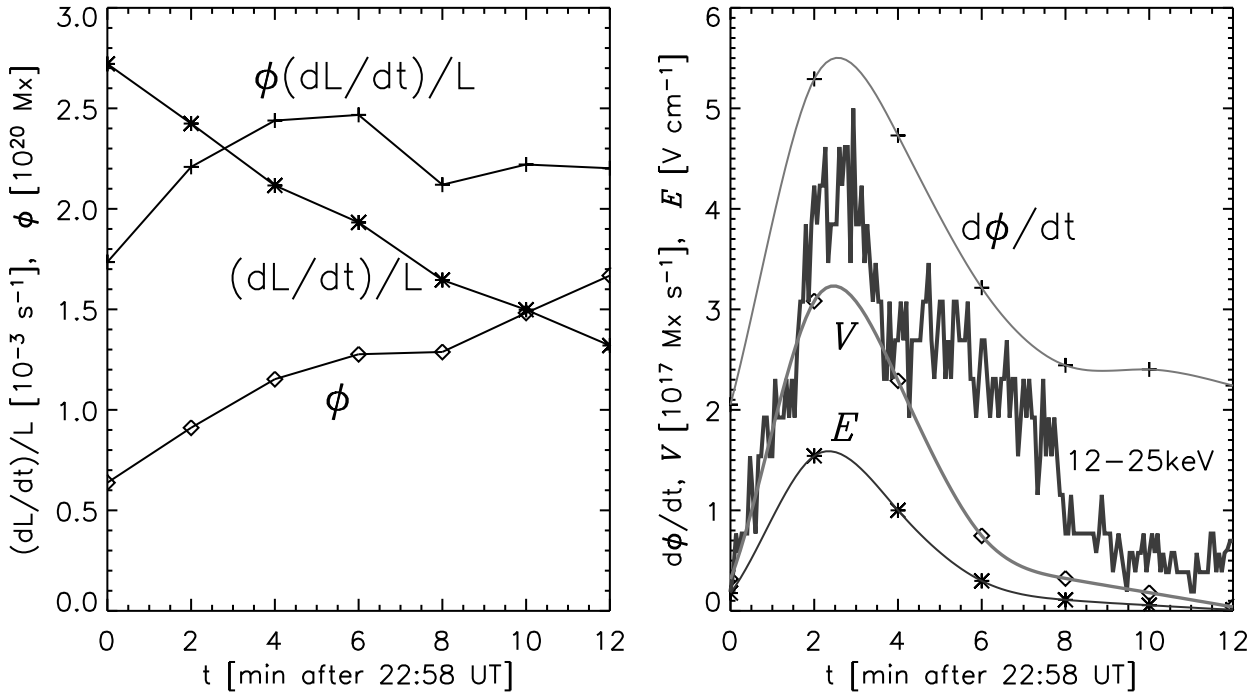

Fig. 5.— Parameters related to the magnetic reconnection during the flare. *Left*: Logarithmic length change rate, $\dot{l}/l$, magnetic flux ϕ and the correction term $(\dot{l}/l)\phi$ are shown as functions of sxce. *Right*: The flux change rate, $\dot{\phi}$, the electric voltage, V, and electric field, E, are shown for comparison.